01 Jan 2017

Boosting the Electrochemical Performance of $Li_{1.2}Mn_{0.54}Ni_{0.13}Co_{0.13}O_2$ by Atomic Layer-Deposited CeO_2 Coating

Yan Gao

Rajankumar L. Patel

Kuan-Yu Shen

Xiaofeng Wang

et. al. For a complete list of authors, see https://scholarsmine.mst.edu/che_bioeng_facwork/521

Recommended Citation

Y. Gao et al., "Boosting the Electrochemical Performance of $Li_{1.2}Mn_{0.54}Ni_{0.13}Co_{0.13}O_2$ by Atomic Layer-Deposited CeO_2 Coating," *ACS Omega*, vol. 3, no. 1, pp. 906-916, American Chemical Society (ACS), Jan 2017.

The definitive version is available at https://doi.org/10.1021/acsomega.7b01922

ACS OMEGA

Article

Cite This: ACS Omega 2018, 3, 906−916

Boosting the Electrochemical Performance of $Li_{1.2}Mn_{0.54}Ni_{0.13}Co_{0.13}O_2$ by Atomic Layer-Deposited CeO_2 Coating

Yan Gao,[†] Rajankumar L. Patel,[†,§] Kuan-Yu Shen,[‡] Xiaofeng Wang,[†] Richard L. Axelbaum,[‡] and Xinhua Liang*[,†]

[†]Department of Chemical and Biochemical Engineering, Missouri University of Science and Technology, Rolla, Missouri 65409, United States

[‡]Department of Energy, Environmental and Chemical Engineering, Washington University in St. Louis, One Brookings Drive, St. Louis, Missouri 63130, United States

Supporting Information

ABSTRACT: It has been demonstrated that atomic layer deposition (ALD) provides an initially safeguarding, uniform ultrathin film of controllable thickness for lithium-ion battery electrodes. In this work, CeO_2 thin films were deposited to modify the surface of lithium-rich $Li_{1.2}Mn_{0.54}Ni_{0.13}Co_{0.13}O_2$ (LRNMC) particles via ALD. The film thicknesses were measured by transmission electron microscopy. For electrochemical performance, ∼2.5 nm CeO_2 film, deposited by 50 ALD cycles (50Ce), was found to have the optimal thickness. At a 1 C rate and 55 °C in a voltage range of 2.0−4.8 V, an initial capacity of 199 mAh/g was achieved, which was 8% higher than that of the uncoated (UC) LRNMC particles. Also, 60.2% of the initial capacity was retained after 400 cycles of charge−discharge, compared to 22% capacity retention of UC after only 180 cycles of charge−discharge. A robust kinetic of electrochemical reaction was found on the CeO_2-coated samples at 55 °C through electrochemical impedance spectroscopy. The conductivity of 50Ce was observed to be around 3 times higher than that of UC at 60−140 °C. The function of the CeO_2 thin-film coating was interpreted as being to increase substrate conductivity and to block the dissolution of metal ions during the charge−discharge process.

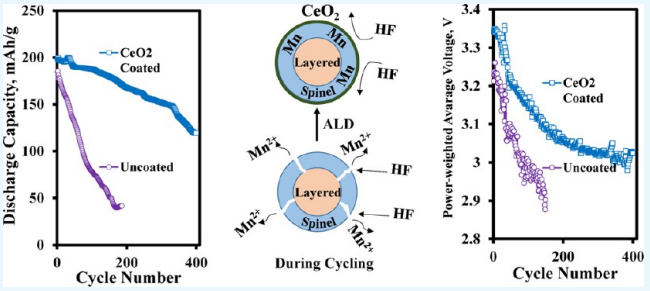

INTRODUCTION

Lithium (Li)-rich layered cathodes have been attracting great interest due to their abundant Li storage and high energy density.[1−5] Their composition is based on a layered structure, with layer−layer integration of two components, $LiMO_2$ (M = Mn, Ni, Co, etc.) and Li_2MnO_3.[3,6] Compared to conventional cathode oxides, such as $LiCoO_2$, $LiMn_2O_4$, and $LiFePO_4$, the advantages of Li-rich layered cathodes include sufficiently high initial capacity (>250 mAh/g), high operating voltage (3.5 V vs Li/Li^+ on average, up to 4.8 V), and low cost with less toxicity.[7−9] However, some drawbacks must be overcome before its commercial utilization, including poor cyclic performance and voltage decay,[7,10−12] limited rate capability resulting from low conductivity, and the formation of a solid electrolyte interface (SEI) layer on the cathode surface.[2,13] During an initial charge to ∼4.5 V, an irreversible reaction of $Li_2MnO_3 \rightarrow Li_2O + MnO_2$ occurs, and Li^+ extracted from Li_2MnO_3 later reinserts into the electrochemically active MnO_2 phase to form a rocksalt $LiMnO_2$ structure.[1,10,14] An unstable $LiMnO_2$ phase, however, will transfer to a spinel-like phase during repeated charge−discharge cycles,[2,14−19] and this will exaggerate the dissolution of transition-metal cations and thicken the SEI layer,[15,20,21] finally leading to further degradation of capacity.

Surface modification has been demonstrated to protect the cathode surface and achieve a better cycle lifetime, such as oxides (e.g., Al_2O_3,[4] TiO_2,[22] MgO,[21] Er_2O_3,[23] SnO_2[24]), fluorides (e.g., CaF_2,[15,25] NH_4F,[11] AlF_3[26,27]), and phosphates (e.g., $AlPO_4$,[28] $FePO_4$[29]). Chen et al.[24] reported that SnO_2-coated $Li_{1.2}Mn_{0.54}Ni_{0.13}Co_{0.13}O_2$ (LRNMC) showed increased cycling stability during 100 cycles of charge−discharge at 600 mA/g and 60 °C. Wang et al.[29] used amorphous $FePO_4$ coating to improve the capacity retention of $Li_{1.2}Mn_{0.54}Ni_{0.13}Co_{0.13}O_2$ from 84.9% of a pristine sample to 95.0% during 100 cycles of charge−discharge at 100 mA/g and room temperature. Liquid-based methods were used for film coatings in all previously mentioned reports. Surface-modified Li-rich layered cathodes showed impressive capacity; however, most of the studies were still within limited cycles of charge−discharge, or only at room temperature, which are not enough to prove the protective effect of coating during a long cycle range and under harsh conditions. At an elevated temperature, the capacity of a Li-rich layered cathode increased,[12,22] but this was accompanied by worse deterioration of capacity.[22,30] Faced with the above-

Received: December 10, 2017
Accepted: January 10, 2018
Published: January 24, 2018

DOI: 10.1021/acsomega.7b01922
ACS Omega 2018, 3, 906−916

mentioned challenges, an ionically and electronically conductive coating of optimal thickness should be effective in protecting the surfaces of the cathode particles.

Atomic layer deposition (ALD) has been demonstrated to be a promising technique for the enhancement of cyclic performance of Li-ion batteries.[30−34] Different from conventional coating methods, ALD can provide precise control of film thicknesses, which is extremely helpful in identifying an optimal thickness. According to our previous work, a CeO_2 ALD coating of optimal thickness successfully solved the trade-off between capacity and cyclic stability for spinel cathodes.[31,33] Surface modification of $Li(Li_{0.17}Ni_{0.2}Co_{0.05}Mn_{0.58})O_2$ by CeO_2 nanoparticles was adopted in other works, but the coating was not conformal and the cyclic number and test at only room temperature were not sufficient to show significant enhancement of cyclic stability.[35] In a previous work, Al_2O_3 ALD-coated $Li_{1.2}Mn_{0.54}Ni_{0.13}Co_{0.13}O_2$ was demonstrated to deliver a higher capacity retention, but lower specific capacity; TiO_2 ALD coating increased the capacity of $Li_{1.2}Mn_{0.54}Ni_{0.13}Co_{0.13}O_2$, but without any mitigation of capacity loss.[30] Herein, ultrathin CeO_2 films of different thicknesses were deposited on the surface of Li-rich $Li_{1.2}Mn_{0.54}Ni_{0.13}Co_{0.13}O_2$ primary particles by ALD. CeO_2 coating of 50 cycles was found to be the optimal thickness for the highest improvement in capacity (∼199 mAh/g) and a ∼60.2% capacity retention, even after 400 cycles of charge−discharge in a voltage range of 2.0−4.8 V at a 1 C rate and 55 °C. This film acted as a conductive barrier to prevent metal dissolution and to lower resistivity of the substrate.

RESULTS AND DISCUSSION

Characterization. The pristine $Li_{1.2}Mn_{0.54}Ni_{0.13}Co_{0.13}O_2$ particles, as shown in Figure 1, were polydispersed spherical

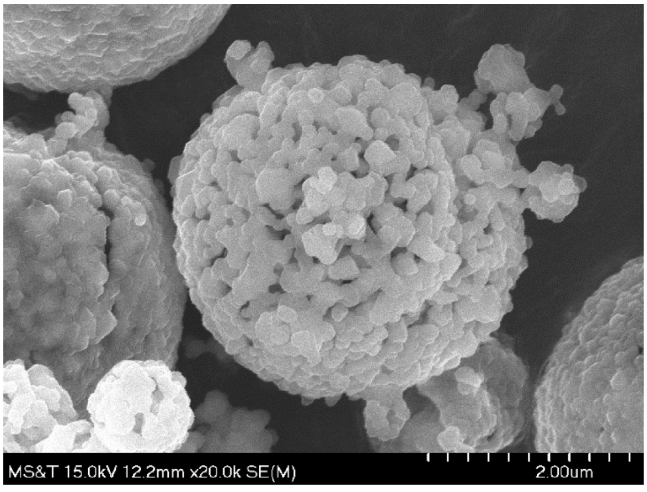

Figure 1. SEM image of pristine LRNMC particles before ALD.

and porous particles, with diameters of 1−3 μm, which were confirmed by scanning electron microscopy (SEM) and found to be consistent with the previously reported work.[30,36] In Figure S1, X-ray diffraction (XRD) patterns of pristine LRNMC particles also confirmed the consistency with previous work.[36]

Various cycles of CeO_2 ALD were deposited on the surface of LRNMC particles, including 30, 50, 70, and 100 cycles (named as 30Ce, 50Ce, 70Ce, and 100Ce, respectively). The purpose was to acquire CeO_2 coatings of different thicknesses because there was a trade-off to solve by controlling the film thickness. Figure 2a shows a transmission electron microscopy

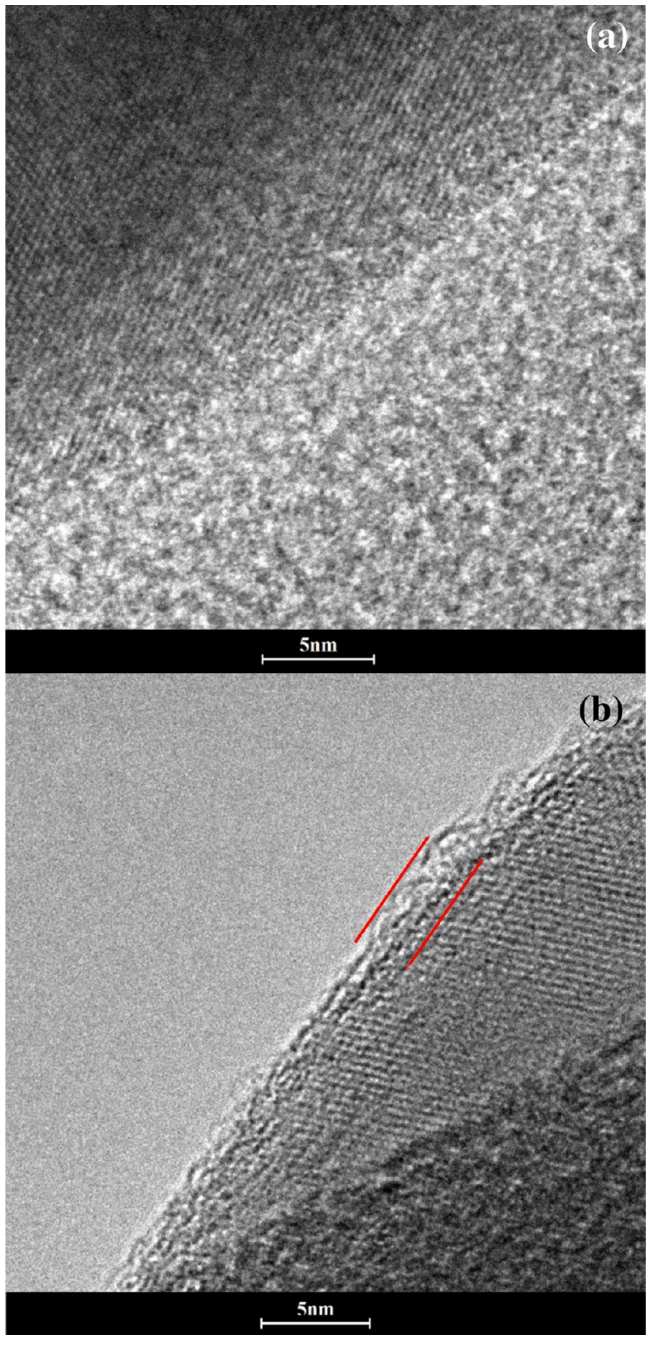

Figure 2. TEM images of (a) UC and (b) 50 cycles CeO_2 ALD-coated LRNMC.

(TEM) image of part of one uncoated (UC) particle, and the edges defined by equidistant fringes can be observed as the smooth surface of the layered cathode. In Figure 2b, an amorphous and conformal layer deposited by 50 cycles of CeO_2 ALD appeared on the particle surface, which can be defined by the crystal structure of LRNMC. The thickness of the film was observed to be ∼2.5 nm. In our previous work,[31] with 50 cycles of CeO_2 ALD, the film thickness was 2.5−3 nm, and with 100 cycles of CeO_2 ALD, the film thickness was ∼5 nm. The growth rate of CeO_2 ALD film was found to be constant. In this work, the film thicknesses were consistent with our previous

DOI: 10.1021/acsomega.7b01922
ACS Omega 2018, 3, 906−916

measurements.[31,33] In addition, surface areas of the UC and 100Ce samples were measured as 7.2 and 7.6 m^2/g, respectively, which indicated that CeO_2 ALD coating did not affect the surface areas of the LRNMC particles.

Electrochemical Analysis. During galvanostatic charge and discharge, all coin cells were tested in a wide voltage range of 2.0−4.8 V. Initial charge−discharge at a 0.05 C (1 C = 250 mA/g) rate and room temperature was performed, as shown in Figure S2. The UC delivered ∼275 mAh/g discharge capacity after the activation of Li_2MnO_3 in the first charge. Slight increases in the discharge capacity of 30Ce, 50Ce, and 70Ce were observed, which were ∼280, ∼284, and ∼279 mAh/g, respectively. This could be attributed to the improvement in conductivity of LRNMC particles by CeO_2 coating. However, the discharge capacity of 100Ce was ∼271 mAh/g, suggesting that the capacity would be lowered if the coating film was too thick. Coulombic efficiencies exhibited ∼83.3, ∼83.8, ∼83.3, ∼83.5, and ∼83.1% for UC, 30Ce, 50Ce, 70Ce, and 100Ce during the initial charge−discharge cycle. These results did not show obvious differences, indicating that the coating material did not affect the activation of Li_2MnO_3. On the other hand, these results also ensured their consistency with the results of previous work.[30] In Figure 3, the rate capabilities of UC, 30Ce, 50Ce, 70Ce, and 100Ce were explored at different C rates (0.1, 0.2, 0.5, 1, and 2 C). At room temperature (Figure 3a), 30Ce, 50Ce, and 70Ce showed initial discharge capacities of ∼250, ∼261, and ∼257 mAh/g at a 0.1 C rate, respectively, which were higher than ∼246 mAh/g of UC and ∼242 mAh/g of 100Ce. This improvement should be attributed to the better conductivity of the CeO_2-coated particles. However, a thicker film would intensify the polarization behavior, as the initial capacity of 100Ce was lower than that of the UC sample. For 30Ce, there was only an increase of ∼4 mAh/g, compared to that of the UC, due to the inadequate thickness of the ionically conductive CeO_2 film. At a 2 C rate, 50Ce delivered an ∼130 mAh/g capacity, which was still the highest, compared to only ∼111 mAh/g for the UC. In Figure S3a, the normalized discharge capacity of Figure 3a is plotted against the discharge capacity at a 0.1 C rate. At a 2 C rate, 50Ce had a capacity that was 50% of the capacity at a 0.1 C rate, but only ∼45% for UC. After the current density returned to 0.1 C, a good reversible capacity was observed for both uncoated and coated samples.

In Figure 3b, the initial capacities of all samples increased at 55 °C because the conductivity of LRNMC had been enhanced at elevated temperatures, which agreed with other works.[12,22,30] At a 0.1 C rate, the 50Ce delivered a higher capacity of ∼270 mAh/g than the ∼255 mAh/g average for the UC. It is worth pointing out that the 100Ce showed an increase of ∼18 mAh/g over the initial capacity at room temperature. Even though the coating was thick, 100Ce seemed to benefit more from a higher temperature than the other coated samples did. Further discussion will be continued as a part of impedance analysis. In Figure S3b, the normalized discharge capacities of coated samples at 55 °C also exhibited improvement in rate capability over those at room temperature. For a 2C rate, the highest increase of ∼5.8% in capacity was observed for 50Ce, but a ∼5% decrease occurred for UC. As the temperature increased, the decomposition of electrolyte at high voltage and hydrogen exchange could have been more frequent and aggravated a hydrogen fluoride (HF) attack. After coin cells were cycled again, at a 0.1 C rate, the reversibility of the initial capacity of UC was not as good as that at room temperature. On the contrary, the reversible capacity was ∼100% for 50Ce and 70Ce

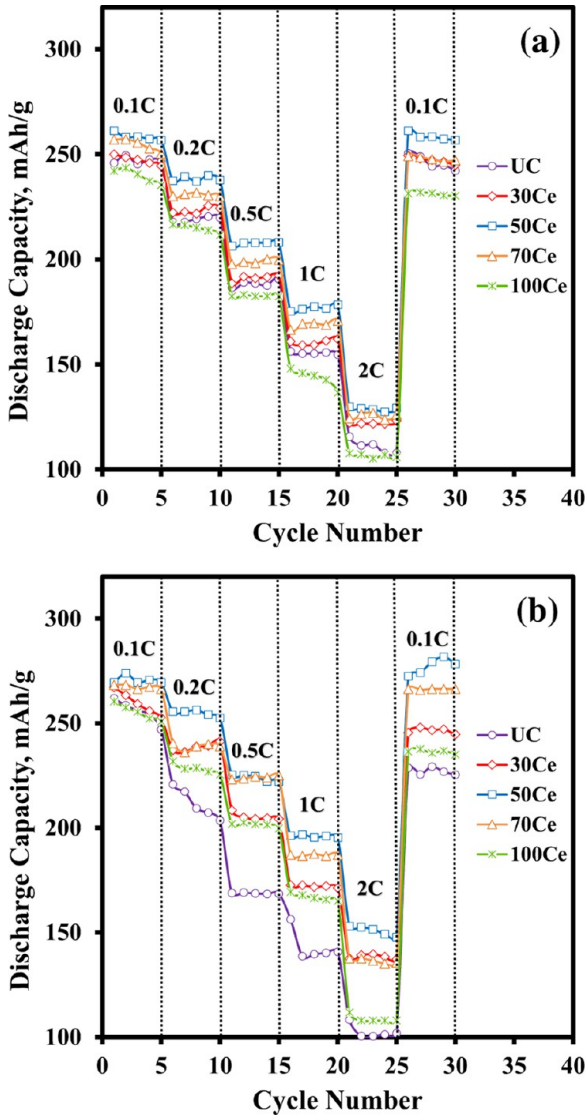

Figure 3. Galvanostatic discharge capacities of coin cells made of UC and different cycles of CeO_2 ALD-coated LRNMC particles at different C rates (0.1, 0.2, 0.5, 1, and 2 C) in the voltage range of 2.0−4.8 V at (a) room temperature and (b) 55 °C.

because the CeO_2 coating was not only protective and prevented the formation of an insulating SEI layer, but also conductive and assisted the charge transfer.

To further investigate and determine the cyclic performance, different coin cells were employed to conduct the galvanostatic cycling test at 1 or 2 C rates. As shown in Figure 4a, for a 1 C rate at room temperature, the initial capacity of 50Ce delivered the highest capacity of ∼166 mAh/g, which was ∼8% higher than the ∼153 mAh/g of UC. The initial capacity of 100Ce was ∼109 mAh/g, but its stable value raised to ∼146 mAh/g because a CeO_2 film of 100 cycles of CeO_2 ALD was too thick. The same phenomena were also observed in other works using Al_2O_3 ALD coating.[37,38] As the charge−discharge cycle proceeded, the capacity of the UC gradually faded and, after 100 cycles, only ∼90 mAh/g were retained. This was ∼58.2% of the initial discharge capacity. The capacity retention rates (with respect to ∼146 mAh/g) of coated LRNMC were ∼92, ∼94.6, ∼93.1, and 95.3% for 30Ce, 50Ce, 70Ce, and 100Ce after 100 cycles of charge−discharge, respectively. In Figure S4, the

DOI: 10.1021/acsomega.7b01922
ACS Omega 2018, 3, 906−916

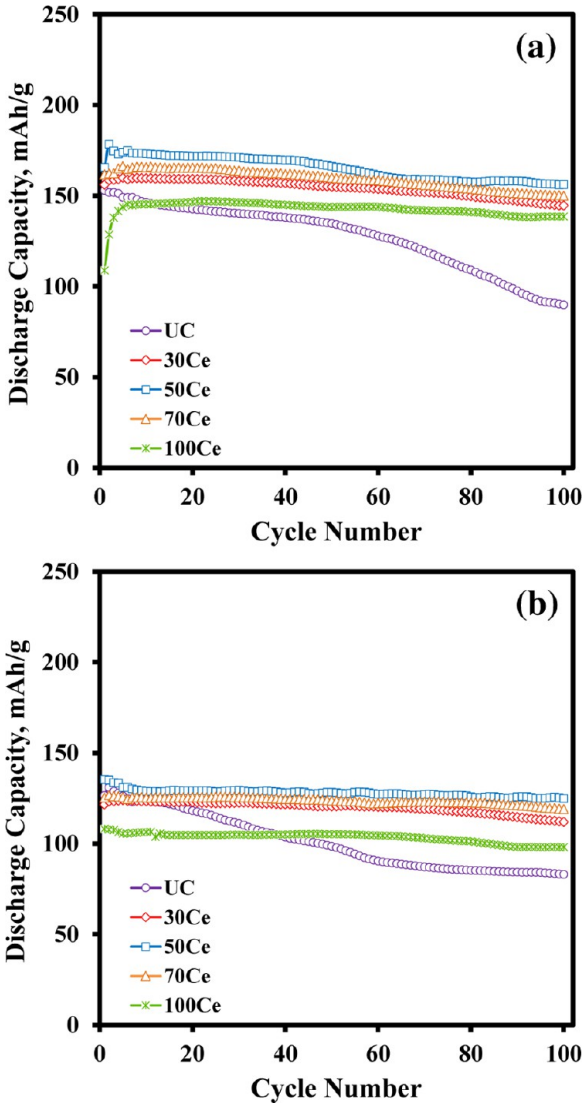

Figure 4. Galvanostatic discharge capacities of coin cells made of UC and different cycles of CeO_2 ALD-coated LRNMC particles at (a) 1 C and (b) 2 C rates in a voltage range of 2.0−4.8 V at room temperature.

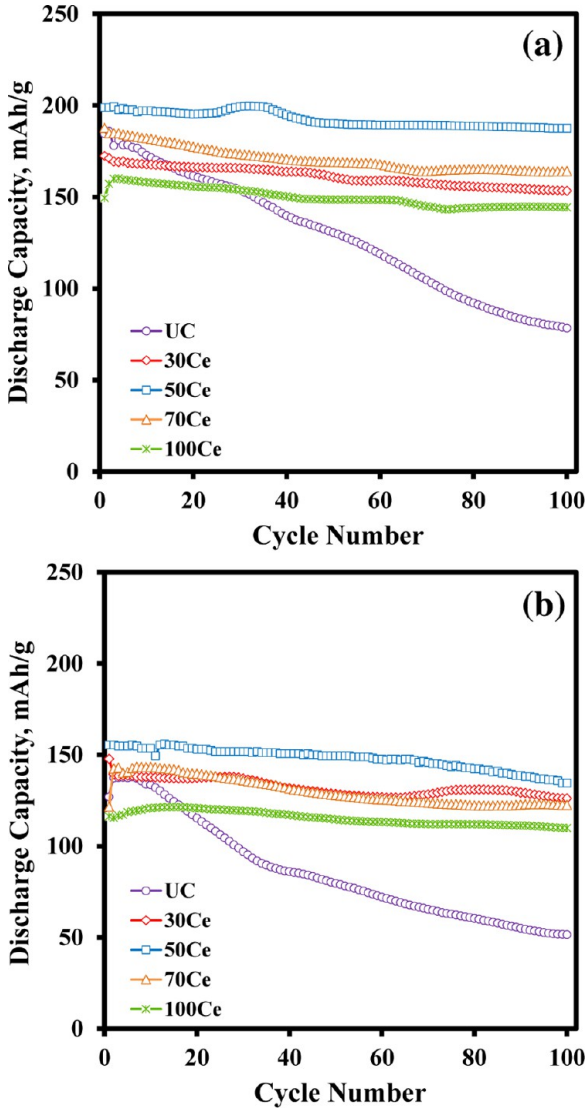

Figure 5. Galvanostatic discharge capacities of coin cells made of UC and different cycles of CeO_2 ALD-coated LRNMC particles at (a) 1 C and (b) 2 C rates in a voltage range of 2.0−4.8 V at 55 °C.

voltage−capacity curves of UC and 50Ce also showed obvious improvement in capacity retention by CeO_2 ALD coating. A remarkable enhancement of cyclic performance was also observed at a 2 C rate (Figure 4b). The initial capacities showed a small increase of 50Ce, compared to UC, whereas in terms of capacity retention (after 100 cycles of charge−discharge), ∼64.3% of UC was in marked contrast to ∼92.4% of 50Ce and 93.3% of 70Ce. In addition, in this work, capacity retention was favored by a higher C rate at room temperature, which agreed well with another work.[39] This suggested that transition-metal ions remain at higher oxidation states due to less Li^+ insertion at higher C rates, thereby alleviating Jahn−Teller distortion.[39]

A comprehensive study of the benefits of CeO_2 ALD coating also involved a cycling test at 55 °C, as shown in Figure 5. At a 1 C rate (Figure 5a), 50Ce delivered ∼199 mAh/g capacity in the first cycle, which was ∼8% higher than ∼184 mAh/g of UC. The initial capacities of 30Ce, 70Ce, and 100Ce were ∼173, ∼188, and ∼150 mAh/g, respectively. If we consider the increment of capacity at an elevated temperature, notably, 100Ce showed a larger capacity increment (i.e., ∼37.6%) than ∼19.8% for 50Ce. The capacity of 100Ce increased to 160 mAh/g after only two cycles of charge and discharge, which was shorter at 55 °C than that at room temperature. This may imply that the kinetic of electrochemical reaction that occurred on the surface of coated samples had been favored at a higher temperature. After 100 cycles of charge−discharge, there was only 42.3% of the initial capacity remaining for UC, suggesting that higher temperature also exacerbated capacity degradation. Accordingly, temperature should simultaneously improve the activity of both electrochemical reactions and side reactions at the electrode−electrolyte interface so that side products (e.g., HF) will intensify their attack on the surface of the electrode.[40] Under the same conditions, 50Ce appeared to scavenge HF and to significantly improve cyclic stability, with a capacity retention of 94.3% after 100 cycles. A previous study indicated that MgO-coated LRNMC, prepared by the melting impregnation method, exhibited 94.3% capacity retention after 50 cycles at 200 mA/g and 60 °C, but the specific capacity of LRNMC was lowered by MgO due to its insulating feature.[21] Similarly, at a 2 C rate (as shown in Figure 5b), the protection of CeO_2 coating contributed to a higher capacity retention. For UC, 30Ce,

DOI: 10.1021/acsomega.7b01922
ACS Omega 2018, 3, 906−916

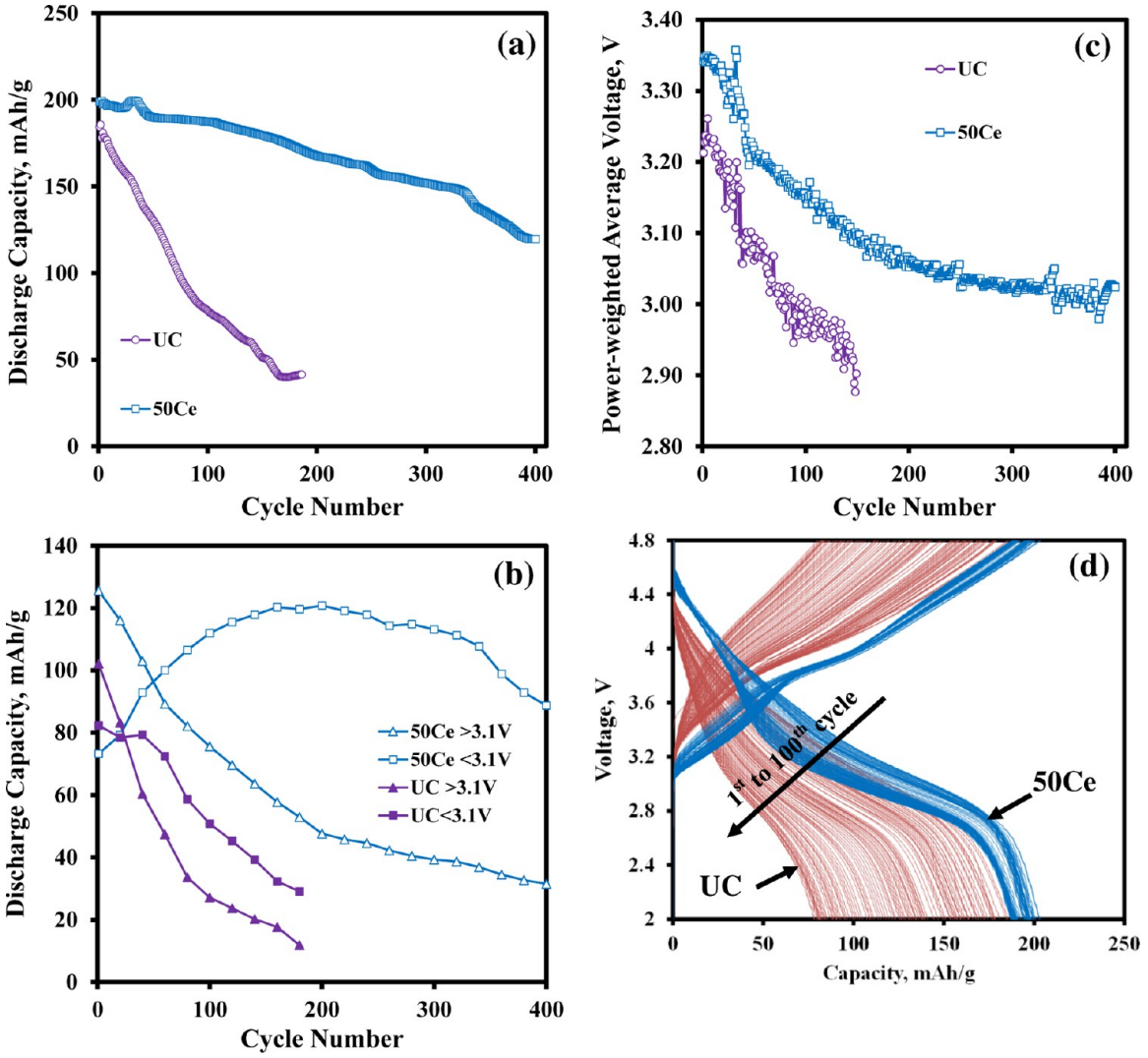

Figure 6. (a) Galvanostatic discharge capacities of UC and 50Ce at a 1 C rate in a voltage range of 2.0−4.8 V for 400 cycles at 55 °C. (b) Separated discharge capacities for the UC and 50Ce at a 1 C rate in a range of 2.0−3.1 V (spinel) and 3.1−4.8 V (layered) at 55 °C. (c) Power-weighted average voltage profiles of the UC in 150 charge−discharge cycles and the 50Ce in 400 charge−discharge cycles under the same conditions. (d) Voltage−capacity curves of UC and 50Ce from 1st to 100th charge−discharge cycle at a 1 C rate in a range of 2.0−4.8 V at 55 °C.

50Ce, 70Ce, and 100Ce, after 100 cycles, the capacity retentions were ∼36.7, ∼84.8, ∼86.6, ∼85.2, and ∼90.8%, respectively. Chen et al. modified the surface of LRNMC by SnO_2, and the coated sample delivered only 68% capacity retention after 100 cycles of charge−discharge at 600 mA/g and 60 °C.[24] The thicker CeO_2 coating of 100Ce showed its exceptional safeguard stability, but the initial capacity was only ∼116 mAh/g at a 2 C rate, compared to ∼156 mAh/g for 50Ce, indicating that 100 cycles of CeO_2 ALD were too thick. In other words, 50Ce would be the optimal thickness for addressing the trade-off between protection and the transport barrier.

To further understand the function of a CeO_2 coating, deeper charge−discharge cycling tests of UC and 50Ce were conducted at a 1 C rate and 55 °C. As shown in Figure 6a, after 180 cycles, UC was found to maintain only ∼22% of its initial capacity. In contrast, with promotion of 50Ce, the reversible capacity was ∼60.2% of its initial capacity, even after 400 cycles of charge−discharge. In our previous reports,[31,33] the cycling life of $LiMn_2O_4$ and $LiMn_{1.5}Ni_{0.5}O_4$ had been significantly extended to 1000 cycles through ALD coating of CeO_2. In view of this, we separated the discharge capacities in Figure 6a into two parts, ">3.1 V" and "<3.1 V", to correspond to each working potential of layered (above 3.1 V) and spinel (below 3.1 V),[5,12,39] to investigate and determine the capacity degradation of the UC and 50Ce. As shown in Figure 6b, capacity was dominantly provided by a spinel structure formed during continuous cycles that were working below ∼3.1 V (also see Figure 6d). The capacities provided by a layered structure kept decreasing, whether for the UC from ∼102 to ∼12 mAh/g in 180 cycles or for 50Ce from ∼126 to ∼32 mAh/g in 400 cycles. It should be related to the structure transition from the layered to a spinel-like phase in LRNMC during its repeated charge−discharge cycling.[15,16,19] Accompanied by the migration of transition-metal cation into Li vacant sites,[12,19,41] the working voltage inevitably decayed. Nevertheless, substituting a spinel-like structure continued to supply a host matrix for Li^+ insertion and disinsertion; thus, it was observed that the capacity of 50Ce increased from ∼73 to ∼120 mAh/g for the <3.1 V section. In Figure 6c, discharge voltage profiles were plotted as power-weighted average voltage versus cycle number, as presented elsewhere.[42] The voltage profiles of 50Ce showed

DOI: 10.1021/acsomega.7b01922
ACS Omega 2018, 3, 906−916

~0.25 V decrease after 150 cycles of charge−discharge, and a slower decrease trend was observed after about 150 cycles of charge−discharge, which also corresponded to the trend of its capacity increase for the <3.1 V section. After 150 cycles, the power-weighted average voltage of the UC decreased by ~0.31 V, from ~3.21 to ~2.90 V, indicating the loss of both layered and spinel structures. CeO_2 film prevented metal dissolution, and the capacity was largely retained, even at a high temperature. Without suppression by a CeO_2 coating, the UC suffered from severe dissolution of host cation and thus the capacity of both >3.1 and <3.1 V parts significantly dropped.

To shed light on the impact of CeO_2 ALD coating, coin cells tested at a 1 C rate were characterized by electrochemical impedance spectroscopy (EIS) before and after their cycling tests at room temperature and 55 °C. All of the EIS data were collected at an open-circuit voltage (OCV) of coin cells when they were fully discharged. Impedance spectroscopy was carried out by applying alternating current (AC) with logarithmically decreasing frequency (from 1 MHz to 1 mHz). In a typical Nyquist plot, the valuable information involves ohmic resistance (R_Ω), the first intersection between curve and real axis (Z' axis), film impedance (R_f/CPE_f), the first semicircle, charge-transfer impedance (R_{ct}/CPE_{ct}), the second semicircle, and Warburg impedance (W_s), the "tail".[43] CPE stands for a constant phase element that is typically explained as double-layer capacitance. Cyclic performance largely depends on the polarization behavior of the electrodes, which can be represented by the sum of R_f and R_{ct}. Separately, R_f characterizes resistance of the surface layers, including a deposited coating and an SEI layer; R_{ct} reflects charge-transfer resistance, suggesting the activity of electrochemical reactions; and the Warburg element stands for mass-transfer resistance for Li^+ from the particle surface toward its center.[43] The model in Figure 7c was applied to fit the collected data and obtain the quantified results listed in Tables 1 and 2. Typically, it really portrays the kinetic inside of the coin cells, but it is still an assumed model without critical physical meaning. The CeO_2 coating aimed to control the thickening of the SEI layer, while preventing dissolution of cation and increasing conductivity.[44]

In Figure 7a, EIS was carried out at room temperature after the initial formation of the coin cells. R_f of the coated LRNMC was positively correlated as an increase in the thickness of the coating, whereas the UC had a higher R_f, indicating that a thicker SEI layer had formed on the surface of the uncoated LRNMC after its formation. For charge-transfer resistance, R_{ct} of the UC was extraordinarily higher than that of the coated samples, 1289 Ω compared to 480, 351, 454, and 796 Ω for 30Ce, 50Ce, 70Ce, and 100Ce, respectively. Therefore, 50Ce had shown the highest activity of electrochemical reaction among all of the samples. In light of Warburg impedance, mass transfer was also favored by the CeO_2 coating. Nevertheless, because 30Ce was not thick enough and provided a higher mass-transfer resistance, it had a lower initial capacity than that of the 50Ce during the cycling test. Besides, most samples had an overlap between R_{ct} and W_s after 100 cycles of charge and discharge, except 50Ce, which showed an apparent "tail" due to its lowest R_{ct}. After 100 charge−discharge cycles, R_Ω and R_f of 30Ce, 50Ce, and 70Ce changed slightly due to protection at the surface, but 100Ce exhibited a higher increase for R_Ω (2.3 Ω) and R_f (20.5 Ω). For the UC, R_f increased by 61.2 Ω, which could be attributed to thickening of the SEI layer. Polarization behavior was clearly pictured as the sum of R_f and R_{ct} (Figure 7d), where 50Ce showed the smallest sum due to its lower R_{ct}

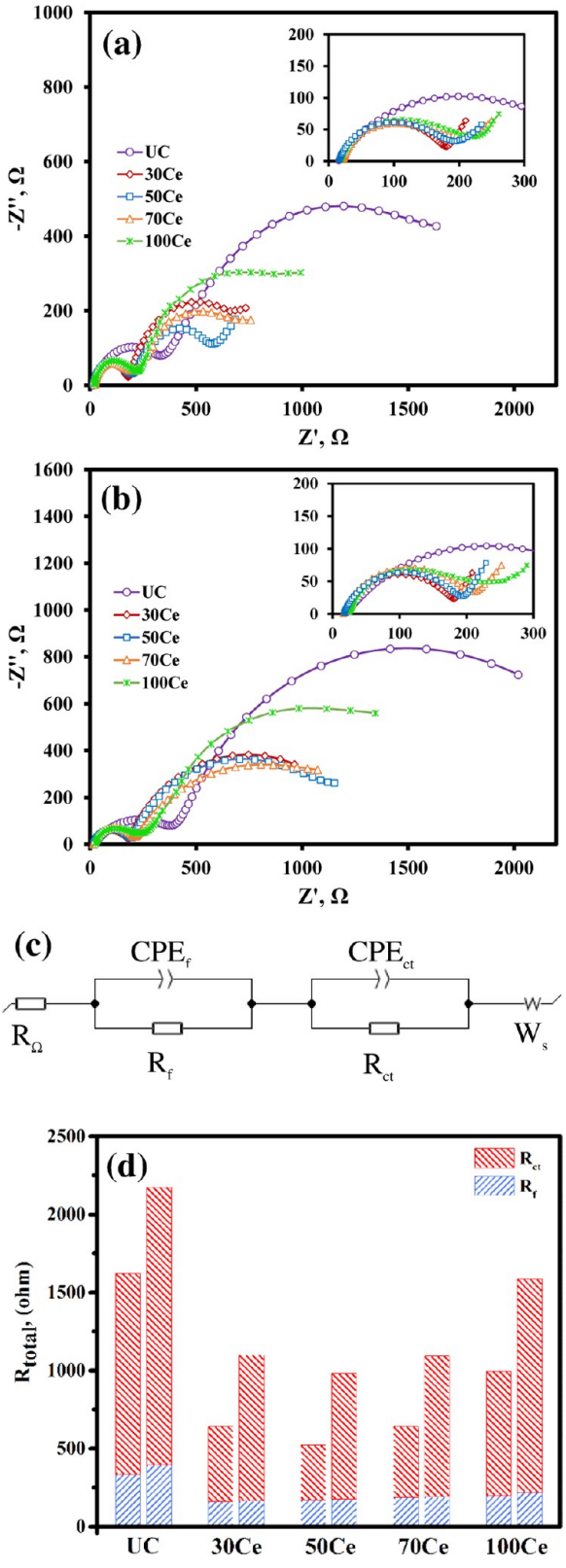

Figure 7. Electrochemical impedance spectra at room temperature for coin cells made of UC and different cycles of CeO_2 ALD-coated LRNMC particles after (a) coin cell formation (0th cycle) and (b) 100th charge−discharge cycle, (c) equivalent circuit for fitting a model of the impedance spectra of coin cells, and (d) summation of fitted parameters, R_f and R_{ct}, at 0th cycle (left) and 100th cycle (right). The inset figures are impedance spectra correspondingly at high-frequency region.

DOI: 10.1021/acsomega.7b01922
ACS Omega 2018, 3, 906−916

Table 1. Impedance Parameters for EIS Data of Coin Cells Tested at Room Temperature

sample	cycle no.	R_Ω (Ω)	R_f (Ω)	R_{ct} (Ω)	C_f (μF)	P_f	C_{ct} (mF)	P_{ct}	W_s (Ω $s^{-1/2}$)
UC	0	14.9	334.0	1289	35.5	0.7	1.5	0.7	47.2
	100	20.0	395.2	1779	62.6	0.6	2.1	0.9	50.3
30Ce	0	16.5	161.8	480	6.0	0.8	1.3	0.8	53.4
	100	16.7	164.2	937	7.3	0.8	1.5	0.8	55.6
50Ce	0	15.8	170.6	351	7.1	0.8	1.4	0.7	40.4
	100	16.8	176.1	808	6.4	0.8	1.1	0.8	46.8
70Ce	0	15.2	187.7	454	11.7	0.8	1.3	0.8	43.2
	100	15.5	190.4	903	7.7	0.8	1.5	0.7	47.5
100Ce	0	17.6	199.4	796	9.4	0.8	1.2	0.8	54.2
	100	19.9	219.9	1367	13.3	0.7	1.5	0.8	61.4

Table 2. Impedance Parameters for EIS Data of Coin Cells Tested at 55 °C

sample	cycle no.	R_Ω (Ω)	R_f (Ω)	R_{ct} (Ω)	C_f (μF)	P_f	C_{ct} (mF)	P_{ct}	W_s (Ω $s^{-1/2}$)
UC	0	12.8	99.1	640	16.9	0.7	1.6	0.5	12.4
	100	12.4	703.4	1724	648	0.5	3.6	0.9	65.3
30Ce	0	9.3	196.8	137	8.3	0.8	0.8	0.8	31.5
	100	8.9	201.9	428	71.5	0.6	1.4	0.8	35.5
50Ce	0	12.3	163.7	85	9.2	0.8	0.9	0.7	27.6
	100	12.7	168.2	380	51.8	0.6	1.8	0.8	32.2
70Ce	0	10.5	174.3	129	11.9	0.8	1.1	0.7	29.1
	100	9.6	185.3	439	243	0.5	1.8	0.7	31.7
100Ce	0	13.3	214.1	167	6.3	0.8	1.0	0.6	27.5
	100	18.6	233.6	525	12.7	0.8	1.5	0.6	50.7

for 351 Ω and supported its highest initial capacity at a 1 C rate. Lower charge-transfer resistance will benefit the formation of an ordered spinel structure and thus enhance the rate capability and capacity retention.[11,15,45]

In Figure 8a, EIS was carried out at 55 °C after formation of coin cells. Compared to resistances at room temperature, samples showed lower values of R_f, R_{ct}, and W_s. At the elevated temperature, higher conductivity and more facile mass transfer led to capacity increase. For the same reason, R_{ct} also decreased considerably for 30Ce, 50Ce, 70Ce, and 100Ce, which were, respectively, 137, 85, 129, and 167 Ω. The W_s values of coated LRNMC at 55 °C were all around 30 Ω, which was lower than 50 Ω at room temperature. However, the formation of the SEI layer at a higher temperature was caused by intensified HF attack and cation dissolution.[31] Thus, the UC showed ∼604 Ω increase of R_f after 100 cycles of charge−discharge, which differed from the small changes in the coated samples. On the other hand, R_{ct} of the UC increased ∼1084 Ω at 55 °C and was much higher than that of the coated samples. This also explained the low capacity retention of UC at 55 °C. Notwithstanding that side reactions became worse at higher temperatures, with the CeO_2 coating protection, a robust kinetic of electrochemical reaction should be helpful in the formation of an ordering spinel phase.[11,15,45] In Figure 8c, the lower sum of R_f and R_{ct} for the coated samples than that for the UC indicated that CeO_2 coating can make LRNMC take full advantage of the augmented capacity at a higher temperature by hindering the worse degradation caused by elevated temperatures. In this case, 50Ce exhibited the lowest resistances of 248.7 and 548.2 Ω before and after cycling tests, respectively, indicating again the optimal thickness for enhancement of the cyclic performance of LRNMC by 50 cycles of CeO_2 ALD coating.

Impedance spectra on particles themselves were measured to understand the function of CeO_2 coating and to estimate conductivity. All samples were made into pellets and characterized by EIS and chronoamperometry (CA). Before the conductivity measurement, XRD was carried out for the pre- and post-annealed samples to make certain that high-temperature annealing did not affect the substrate itself (as shown in Figure S1). The AC impedance spectra (Figure S5) were analyzed using a distinctive equivalent circuit model from coin cell analysis, as shown in Figure 9b. CPE_1 represents the capacitance of geometric configuration between two electronically conducting Ag electrodes. Parallel elements are a series of R & CPE_2 for resistance of the pellet and double-layer capacitance.[46] The conductivity was calculated based on measured resistance R, thickness, and the area of each pellet. In Figure 9a, Arrhenius plots are based on the following equation

$$\sigma = A_0 \exp(-E_a/RT) \quad (1)$$

where σ denotes electronic conductivity, A_0 is the pre-exponential factor, and E_a means activation energy. The conductivity was observed to increase as temperature increased, which was consistent with the cyclic performance of coin cells during cycling tests. Higher conductivity benefits the kinetic of electrochemical reactions and thus coin cells exhibited a lower charge-transfer resistance (Figures 7a and 8a). Also, CeO_2 coating of 30Ce, 50Ce, and 70Ce increased the conductivity of LRNMC particles ∼3 times, compared to that of UC. But the resistance of 100Ce was higher than that of the other coated samples. This behavior can be attributed to the fact that the CeO_2 ALD film of 100 cycles was too thick and the delayed transportation process at the interface increased the charge-transfer resistance. Above 100 °C, the conductivities of 30Ce, 50Ce, and 70Ce almost coincided, which was different from the findings in our previous works, where CeO_2 ALD films were deposited on the spinel.[31,33] However, as the temperature dropped to below 100 °C, there was a small deviation among

DOI: 10.1021/acsomega.7b01922
ACS Omega 2018, 3, 906−916

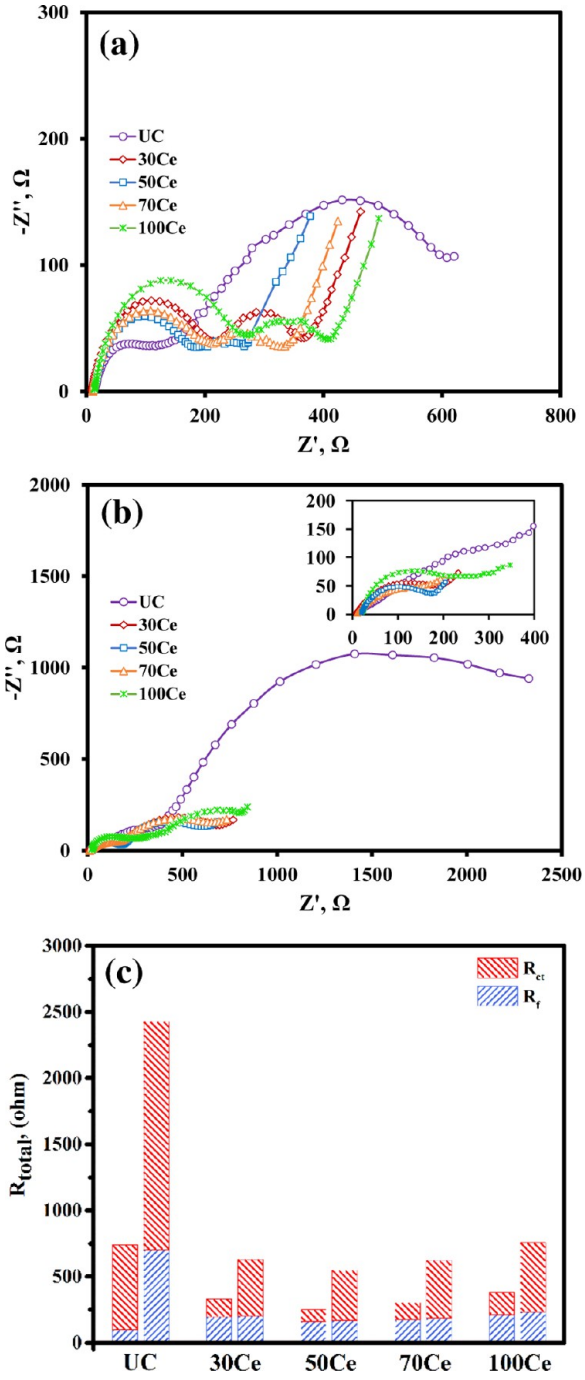

Figure 8. Electrochemical impedance spectra at 55 °C for coin cells made of UC and different cycles of CeO_2 ALD-coated LRNMC particles after (a) coin cell formation (0th cycle), (b) 100th charge−discharge cycle, and (c) summation of fitted parameters, R_f and R_{ct}, at 0th cycle (left) and 100th cycle (right). The inset figure shows impedance spectra at high-frequency regions.

30Ce, 50Ce, and 70Ce; clearly, 50Ce showed the highest conductivity below 100 °C. In light of this trend, we believed that the conductivity of 50Ce should be higher than those of the other samples at lower temperatures; hence, this benefits its cyclic performance so that it was better than that of 30Ce and 70Ce.

In Figure 10, SEM was carried out on both UC and 50Ce cathodes after 400 cycles of charge−discharge at a 1 C rate and 55 °C. The SEM image of UC in Figure 10a shows severe

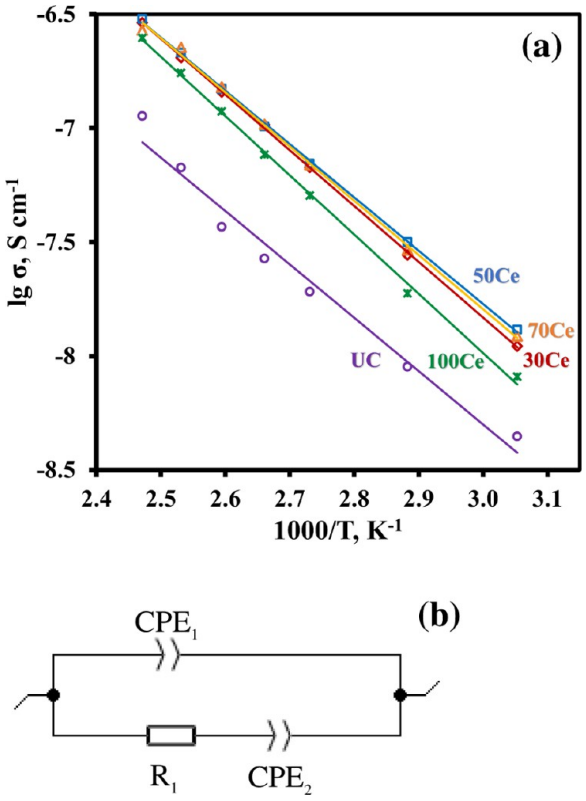

Figure 9. (a) Arrhenius plots of conductivities of pellets made of UC and different cycles of CeO_2 ALD-coated LRNMC particles vs temperatures and (b) equivalent circuit for fitting a model of AC impedance spectra of pellets.

exfoliation and breakup of UC particles in the cathode, which should be the reason for the irreversible loss of its capacity. However, in Figure 10b, 50Ce still mostly maintained its original spherical shape. These results indicated that a CeO_2 coating can effectively scavenge HF to mitigate side reactions with electrolyte and protect the structure of cathode particles.

CONCLUSIONS

The layered structure of LRNMC acquires a good stabilization and excess Li supplement through being composited with the Li_2MnO_3 phase; however, it is also affected by the insulating feature of Li_2MnO_3. The phase transition and metal dissolution cause further degradation of capacity. Hence, in this work, we modified the surface of Li-rich layered cathode $Li_{1.2}Mn_{0.54}Ni_{0.13}Co_{0.13}O_2$ by CeO_2 ALD coating to increase the substrate conductivity and set a barrier for metal dissolution. The optimal CeO_2 film thickness was ∼2.5 nm, deposited by 50 cycles of CeO_2 ALD. With the optimal thickness of a CeO_2 coating, there was ∼8% of initial capacity increase at both room temperature and 55 °C; the cyclic stability of LRNMC improved to ∼60.2% capacity retention after 400 cycles of charge−discharge in a voltage range of 2.0−4.8 V at a 1 C rate and 55 °C. Overall, CeO_2 ALD coating is an effective way to promote the electrochemical performance of cathode particles because of its safeguarding and conductive nature.

EXPERIMENTAL SECTION

CeO_2 ALD Coating. A series of different thicknesses of CeO_2 films were coated on the LRNMC particles by ALD in a

DOI: 10.1021/acsomega.7b01922
ACS Omega 2018, 3, 906−916

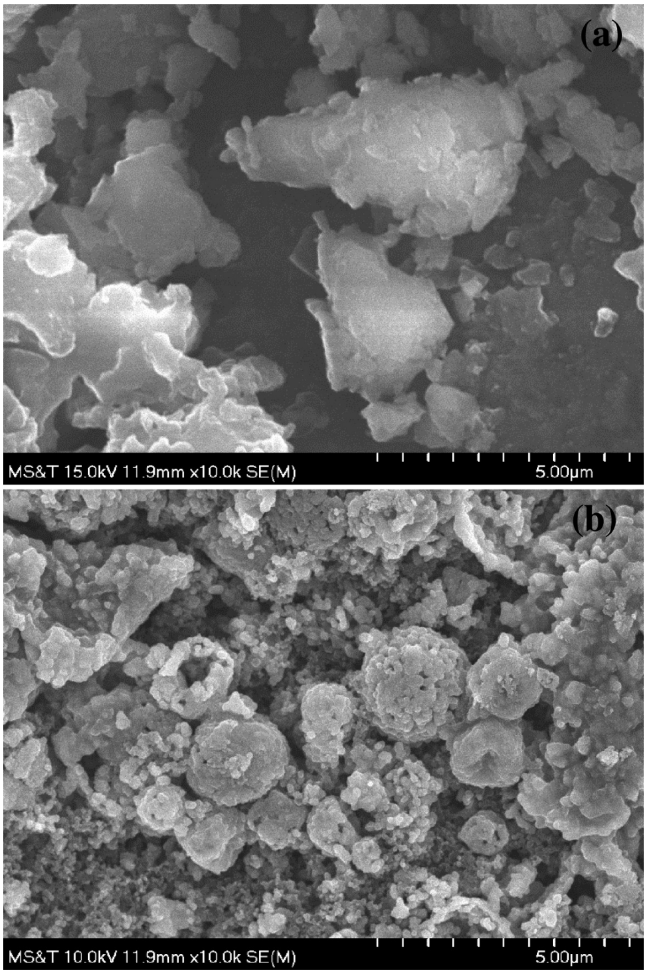

Figure 10. SEM images of (a) UC and (b) 50Ce cathodes after 400 cycles of charge−discharge at a 1 C rate at 55 °C.

fluidized bed reactor (illustrated in detail elsewhere).[47] The LRNMC particles were prepared using a spray pyrolysis process, previously described in detail.[30,36] Tris(*i*-propylcyclopentadienyl)cerium (Ce(*i*PrCp)$_3$) (99.9%, Strem Chemicals) and deionized water were used as precursors for CeO_2 ALD. A typical coating cycle consisted of Ce(*i*PrCp)$_3$ dose, N_2 flush, H_2O dose, and N_2 flush. CeO_2 ALD was carried out at 250 °C. Ce(*i*PrCp)$_3$ was heated in a feed bubbler at ∼140 °C, and N_2 was used as carrier gas for Ce(*i*PrCp)$_3$. All feed lines were maintained at the same temperature to avoid condensation of the precursors. The ALD process was controlled through LABVIEW program. CeO_2 ALD of 30, 50, 70, and 100 cycles was applied to obtain different thicknesses, and named as UC (uncoated samples), 30Ce (30 cycles of CeO_2 ALD-coated LRNMC particles), 50Ce, 70Ce, and 100Ce, respectively.

Coin Cell Assembly. The cathode slurry was prepared by mixing 80 wt % LRNMC particles, 10 wt % Super P carbon black (Alfa Aesar), and 10 wt % poly(vinylidene fluoride) (Sigma-Aldrich) in *N*-methyl-2-pyrrolidone (Sigma-Aldrich) solvent. The slurry was uniformly cast on aluminum foil using a doctor blade (MTI Corp.). The coated foil was then dried in a vacuum oven at 120 °C overnight. After acquiring the dry coated foil, a working electrode was punched into a round disk with a diameter of ∼0.95 cm, loaded with a mass of ∼2.4 mg/cm^2 of active materials. Assembly of CR2032 coin cells was finished in an Ar-filled glovebox. Li metal (99.9% trace-metal basis, Sigma-Aldrich) served as the counter electrode, with separator Celgard 2325 between electrodes. The electrolyte was 1 mol/L $LiPF_6$ solution (Sigma-Aldrich) with a mixed solvent of ethylene carbonate and dimethyl carbonate with a volume ratio of 1:1.

Characterization. A Quantachrome Autosorb-1 was used to obtain nitrogen adsorption and desorption isotherms of the UC and 100Ce samples at −196 °C. The surface area of the particles was calculated using the Brunauer−Emmett−Teller method in a relative pressure range of 0.05−0.25. The UC and 50Ce samples were visualized with an FEI Tecnai F20 field emission gun high-resolution transmission electron microscope. Film thickness was measured on the basis of TEM images. Morphology of pristine LRNMC particles was visualized using a Hitachi S-4700 field emission scanning electrode microscope. UC and 50Ce coin cells were dissembled after a galvanostatic charge−discharge test at a 1 C rate at 55 °C, and their cathodes were investigated by the same SEM equipment. To ensure that most of the parts of each sample was studied (rather than just a localized area), adequate and equal amounts of time were spent on SEM analysis of all samples. X-ray diffraction (XRD) was carried out on a Phillips powder diffractometer, using Cu Kα radiation and λ = 1.5406 Å, at a scan rate of 2°/min and step size of 0.2°.

Electrochemical Analysis. The galvanostatic cycling test was carried out on a battery test station (Neware Corp.) in the voltage range of 2.0−4.8 V at different temperatures (room temperature and 55 °C). The electrochemical impedance spectroscopy (EIS) measurement was carried out using a Biologic impedance analyzer in a frequency range of 1 mHz to 1 MHz with an excitation signal of 10 mV at different temperatures (room temperature and 55 °C). The consistency of open-circuit voltage (OCV) of every tested coin cell was checked to confirm the validity of the EIS data. Conductivity measurement was performed using the same analyzer on active materials at different temperatures (60, 80, 100, 110, 120, 130, and 140 °C). Each sample was first cold-pressed into a round pellet with a diameter of ∼1.3 cm and thickness of ∼0.1 cm and then annealed at 800 °C for 24 h to solidify them. Meanwhile, pristine LRNMC particles were characterized by XRD before and after their annealing operation to make sure that the annealing process would not affect the original structure of LRNMC particles. After that, both sides of the pellets were coated with Ag paste (Sigma-Aldrich), which acted as a blocking electrode. Before measurement, the Ag-coated pellets were dried in a vacuum oven at 120 °C for 1 h. The AC conductivity measurement was performed on pellets using EIS in the frequency range of 1 mHz to 1 MHz with an excitation signal of 50 mV. Then, direct current (DC) conductivity measurement was performed on the same pellets using chronoamperometry (CA) at different voltages of 0.5, 0.75, 1.0, 1.25, and 1.5 V.

■ ASSOCIATED CONTENT

Supporting Information

The Supporting Information is available free of charge on the ACS Publications website at DOI: 10.1021/acsomega.7b01922.

XRD patterns of pristine and annealed uncoated LRNMC particles; initial charge−discharge voltage−capacity profiles of UC and LRNMC particles coated with different cycles of CeO_2 ALD films at a 0.05 C rate at room temperature; normalized discharge capacity of

DOI: 10.1021/acsomega.7b01922
ACS Omega 2018, 3, 906−916

coin cells made of UC and LRNMC particles coated with different cycles of CeO_2 ALD at room temperature and 55 °C; voltage−capacity curves of UC and 50Ce in 100 cycles of charge−discharge at a 1 C rate in a range of 2.0−4.8 V at room temperature; Nyquist impedance spectra of UC and 50Ce pellets at 60−140 °C with corresponding fitting curves; and DC resistances of pellets made of UC and LRNMC particles coated with different cycles of CeO_2 ALD at different temperatures (PDF)

AUTHOR INFORMATION

Corresponding Author

*E-mail: liangxin@mst.edu.

ORCID

Rajankumar L. Patel: 0000-0001-7667-5918

Xiaofeng Wang: 0000-0002-2511-3074

Xinhua Liang: 0000-0001-7979-0532

Present Address

§Energy and Environmental Directorate, Pacific Northwest National Laboratory, Richland, Washington 99354, United States (R.L.P.).

Notes

The authors declare no competing financial interest.

ACKNOWLEDGMENTS

This work was supported in part by the National Science Foundation grant NSF DMR 1464111 and the Energy Research and Development Center (ERDC) at Missouri University of Science and Technology. The authors thank Dr. Jingjing Qing at the Materials Research Center at Missouri University of Science and Technology for the TEM analysis.

REFERENCES

(1) Thackeray, M. M.; Kang, S.-H.; Johnson, C. S.; Vaughey, J. T.; Benedek, R.; Hackney, S. A. Li_2MnO_3-stabilized $LiMO_2$ (M = Mn, Ni, Co) electrodes for lithium-ion batteries. *J. Mater. Chem.* **2007**, *17*, 3112−3125.

(2) Jiang, M.; Key, B.; Meng, Y. S.; Grey, C. P. Electrochemical and structural study of the layered, "Li-excess" lithium-ion battery electrode material $Li[Li_{1/9}Ni_{1/3}Mn_{5/9}]O_2$. *Chem. Mater.* **2009**, *21*, 2733−2745.

(3) Thackeray, M. M.; Johnson, C. S.; Vaughey, J. T.; Li, N.; Hackney, S. A. Advances in manganese-oxide 'composite' electrodes for lithium-ion batteries. *J. Mater. Chem.* **2005**, *15*, 2257−2267.

(4) Wu, Y.; Manthiram, A. High capacity, surface-modified layered $Li[Li_{(1-x)/3}Mn_{(2-x)/3}Ni_{x/3}Co_{x/3}]O_2$ cathodes with low irreversible capacity loss. *Electrochem. Solid-State Lett.* **2006**, *9*, A221−A224.

(5) Lu, Z.; Beaulieu, L. Y.; Donaberger, R. A.; Thomas, C. L.; Dahn, J. R. Synthesis, structure, and electrochemical behavior of $Li-[Ni_xLi_{1/3-2/3x}Mn_{2/3-1/3x}]O_2$. *J. Electrochem. Soc.* **2002**, *149*, A778−A791.

(6) Xu, B.; Fell, C. R.; Chi, M.; Meng, Y. S. Identifying surface structural changes in layered Li-excess nickel manganese oxides in high voltage lithium ion batteries: A joint experimental and theoretical study. *Energy Environ. Sci.* **2011**, *4*, 2223−2233.

(7) Zhang, L.; Jin, K.; Wang, L.; Zhang, Y.; Li, X.; Song, Y. High capacity $Li_{1.2}Mn_{0.54}Ni_{0.13}Co_{0.13}O_2$ cathode materials synthesized using mesocrystal precursors for lithium-ion batteries. *J. Alloys Compd.* **2015**, *638*, 298−304.

(8) Du, C.; Zhang, F.; Ma, C.; Wu, J.; Tang, Z.; Zhang, X.; Qu, D. Synthesis and electrochemical properties of $Li_{1.2}Mn_{0.54}Ni_{0.13}Co_{0.13}O_2$ cathode material for lithium-ion battery. *Ionics* **2016**, *22*, 209−218.

(9) Bai, Y.; Li, Y.; Wu, C.; Lu, J.; Li, H.; Liu, Z.; Zhong, Y.; Chen, S.; Zhang, C.; Amine, K.; Wu, F. Lithium-rich nanoscale $Li_{1.2}Mn_{0.54}Ni_{0.13}Co_{0.13}O_2$ cathode material prepared by co-precipitation combined freeze drying (CP-FD) for lithium-ion batteries. *Energy Technol.* **2015**, *3*, 843−850.

(10) Mohanty, D.; Sefat, A. S.; Kalnaus, S.; Li, J.; Meisner, R. A.; Payzant, E. A.; Abraham, D. P.; Wood, D. L.; Daniel, C. Investigating phase transformation in the $Li_{1.2}Co_{0.1}Mn_{0.55}Ni_{0.15}O_2$ lithium-ion battery cathode during high-voltage hold (4.5 V) via magnetic, X-ray diffraction and electron microscopy studies. *J. Mater. Chem. A* **2013**, *1*, 6249−6261.

(11) Li, L.; Chang, Y. L.; Xia, H.; Song, B. H.; Yang, J. R.; Lee, K. S.; Lu, L. NH_4F surface modification of Li-rich layered cathode materials. *Solid State Ionics* **2014**, *264*, 36−44.

(12) Croy, J. R.; Kim, D.; Balasubramanian, M.; Gallagher, K.; Kang, S.-H.; Thackeray, M. M. Countering the voltage decay in high capacity $xLi_2MnO_3\cdot(1-x)LiMO_2$ electrodes (M = Mn, Ni, Co) for Li^+-ion batteries. *J. Electrochem. Soc.* **2012**, *159*, A781−A790.

(13) Fell, C. R.; Carroll, K. J.; Chi, M.; Meng, Y. S. Synthesis−structure−property relations in layered, "Li-excess" oxides electrode materials $Li[Li_{1/3-2x/3}Ni_xMn_{2/3-x/3}]O_2$ (x = 1/3, 1/4, and 1/5). *J. Electrochem. Soc.* **2010**, *157*, A1202−A1211.

(14) Kim, J.-S.; Johnson, C. S.; Vaughey, J. T.; Thackeray, M. M.; Hackney, S. A.; Yoon, W.; Grey, C. P. Electrochemical and structural properties of $xLi_2M'O_3\cdot(1-x)LiMn_{0.5}Ni_{0.5}O_2$ electrodes for lithium batteries (M′ = Ti, Mn, Zr; $0 \le x \le 0.3$). *Chem. Mater.* **2004**, *16*, 1996−2006.

(15) Liu, X.; Huang, T.; Yu, A. Surface phase transformation and CaF_2 coating for enhanced electrochemical performance of Li-rich Mn-based cathodes. *Electrochim. Acta* **2015**, *163*, 82−92.

(16) Fell, C. R.; Qian, D.; Carroll, K. J.; Chi, M.; Jones, J. L.; Meng, Y. S. Correlation between oxygen vacancy, microstrain, and cation distribution in lithium-excess layered oxides during the first electrochemical cycle. *Chem. Mater.* **2013**, *25*, 1621−1629.

(17) Gu, M.; Belharouak, I.; Zheng, J.; Wu, H.; Xiao, J.; Genc, A.; Amine, K.; Thevuthasan, S.; Baer, D. R.; Zhang, J.-G.; Browning, N. D.; Liu, J.; Wang, C. Formation of the spinel phase in the layered composite cathode used in Li-ion batteries. *ACS Nano* **2013**, *7*, 760−767.

(18) Reed, J.; Ceder, G.; Van Der Ven, A. Layered-to-spinel phase transition in Li_xMnO_2. *Electrochem. Solid-State Lett.* **2001**, *4*, A78−A81.

(19) Boulineau, A.; Simonin, L.; Colin, J.-F.; Bourbon, C.; Patoux, S. First evidence of manganese−nickel segregation and densification upon cycling in Li-rich layered oxides for lithium batteries. *Nano Lett.* **2013**, *13*, 3857−3863.

(20) Edström, K.; Gustafsson, T.; Thomas, J. O. The cathode−electrolyte interface in the Li-ion battery. *Electrochim. Acta* **2004**, *50*, 397−403.

(21) Shi, S. J.; Tu, J. P.; Tang, Y. Y.; Liu, X. Y.; Zhang, Y. Q.; Wang, X. L.; Gu, C. D. Enhanced cycling stability of $Li-[Li_{0.2}Mn_{0.54}Ni_{0.13}Co_{0.13}]O_2$ by surface modification of MgO with melting impregnation method. *Electrochim. Acta* **2013**, *88*, 671−679.

(22) Zheng, J. M.; Li, J.; Zhang, Z. R.; Guo, X. J.; Yang, Y. The effects of TiO_2 coating on the electrochemical performance of $Li-[Li_{0.2}Mn_{0.54}Ni_{0.13}Co_{0.13}]O_2$ cathode material for lithium-ion battery. *Solid State Ionics* **2008**, *179*, 1794−1799.

(23) Zhang, S.; Gu, H.; Tang, T.; Du, W.; Gao, M.; Liu, Y.; Jian, D.; Pan, H. In situ encapsulation of the nanoscale Er_2O_3 phase to drastically suppress voltage fading and capacity degradation of a Li- and Mn-rich layered oxide cathode for Lithium ion batteries. *ACS Appl. Mater. Interfaces* **2017**, *9*, 33863−33875.

(24) Chen, C.; Geng, T.; Du, C.; Zuo, P.; Cheng, X.; Ma, Y.; Yin, G. Oxygen vacancies in SnO_2 surface coating to enhance the activation of layered Li-rich $Li_{1.2}Mn_{0.54}Ni_{0.13}Co_{0.13}O_2$ cathode material for Li-ion batteries. *J. Power Sources* **2016**, *331*, 91−99.

(25) Liu, X.; Liu, J.; Huang, T.; Yu, A. CaF_2-coated $Li_{1.2}Mn_{0.54}Ni_{0.13}Co_{0.13}O_2$ as cathode materials for Li-ion batteries. *Electrochim. Acta* **2013**, *109*, 52−58.

(26) Pang, S.; Wang, Y.; Chen, T.; Shen, X.; Xi, X.; Liao, D. The effect of AlF_3 modification on the physicochemical and electro-

DOI: 10.1021/acsomega.7b01922
ACS Omega 2018, 3, 906−916

chemical properties of Li-rich layered oxide. *Ceram. Int.* **2016**, *42*, 5397−5402.
(27) Zhu, Z.; Cai, F.; Yu, J. Improvement of electrochemical performance for AlF_3-coated $Li_{1.3}Mn_{4/6}Ni_{1/6}Co_{1/6}O_{2.40}$ cathode materials for Li-ion batteries. *Ionics* **2016**, *22*, 1353−1359.
(28) Venkateswara Rao, C.; Soler, J.; Katiyar, R.; Shojan, J.; West, W. C.; Katiyar, R. S. Investigations on electrochemical behavior and structural stability of $Li_{1.2}Mn_{0.54}Ni_{0.13}Co_{0.13}O_2$ lithium-ion cathodes via in-situ and ex-situ Raman Spectroscopy. *J. Phys. Chem. C* **2014**, *118*, 14133−14141.
(29) Wang, Z.; Liu, E.; He, C.; Shi, C.; Li, J.; Zhao, N. Effect of amorphous $FePO_4$ coating on structure and electrochemical performance of $Li_{1.2}Ni_{0.13}Co_{0.13}Mn_{0.54}O_2$ as cathode material for Li-ion batteries. *J. Power Sources* **2013**, *236*, 25−32.
(30) Zhang, X.; Belharouak, I.; Li, L.; Lei, Y.; Elam, J. W.; Nie, A.; Chen, X.; Yassar, R. S.; Axelbaum, R. L. Structural and electrochemical study of Al_2O_3 and TiO_2 coated $Li_{1.2}Ni_{0.13}Mn_{0.54}Co_{0.13}O_2$ cathode material using ALD. *Adv. Energy Mater.* **2013**, *3*, 1299−1307.
(31) Patel, R. L.; Xie, H.; Park, J.; Asl, H. Y.; Choudhury, A.; Liang, X. Significant capacity and cycle-life improvement of lithium-ion batteries through ultrathin conductive film stabilized cathode particles. *Adv. Mater. Interfaces* **2015**, *2*, No. 1500046.
(32) Palaparty, S. A.; Patel, R. L.; Liang, X. Enhanced cycle life and capacity retention of iron oxide ultrathin film coated SnO_2 nanoparticles at high current densities. *RSC Adv.* **2016**, *6*, 24340−24348.
(33) Patel, R. L.; Palaparty, S. A.; Liang, X. Ultrathin conductive CeO_2 coating for significant improvement in electrochemical performance of $LiMn_{1.5}Ni_{0.5}O_4$ cathode materials. *J. Electrochem. Soc.* **2017**, *164*, A6236−A6243.
(34) Patel, R. L.; Jiang, Y.-B.; Choudhury, A.; Liang, X. Employing synergetic effect of doping and thin film coating to boost the performance of lithium-ion battery cathode particles. *Sci. Rep.* **2016**, *6*, No. 25293.
(35) Yuan, W.; Zhang, H. Z.; Liu, Q.; Li, G. R.; Gao, X. P. Surface modification of $Li(Li_{0.17}Ni_{0.2}Co_{0.05}Mn_{0.58})O_2$ with CeO_2 as cathode material for Li-ion batteries. *Electrochim. Acta* **2014**, *135*, 199−207.
(36) Zhang, X.; Axelbaum, R. L. Spray pyrolysis synthesis of mesoporous lithium-nickel-manganese-oxides for high energy Li-ion batteries. *J. Electrochem. Soc.* **2012**, *159*, A834−A842.
(37) Guan, D.; Jeevarajan, J. A.; Wang, Y. Enhanced cycleability of $LiMn_2O_4$ cathodes by atomic layer deposition of nanosized-thin Al_2O_3 coatings. *Nanoscale* **2011**, *3*, 1465−1469.
(38) Guan, D.; Wang, Y. Ultrathin surface coatings to enhance cycling stability of $LiMn_2O_4$ cathode in lithium-ion batteries. *Ionics* **2013**, *19*, 1−8.
(39) Song, B.; Liu, Z.; Lai, M. O.; Lu, L. Structural evolution and the capacity fade mechanism upon long-term cycling in Li-rich cathode material. *Phys. Chem. Chem. Phys.* **2012**, *14*, 12875−12883.
(40) Talyosef, Y.; Markovsky, B.; Salitra, G.; Aurbach, D.; Kim, H.-J.; Choi, S. The study of $LiNi_{0.5}Mn_{1.5}O_4$ 5-V cathodes for Li-ion batteries. *J. Power Sources* **2005**, *146*, 664−669.
(41) Hoang, K. Defect physics, delithiation mechanism, and electronic and ionic conduction in layered lithium manganese oxide cathode materials. *Phys. Rev. Appl.* **2015**, *3*, No. 024013.
(42) Lengyel, M.; Zhang, X.; Atlas, G.; Bretscher, H. L.; Belharouak, I.; Axelbaum, R. L. Composition optimization of layered lithium nickel manganese cobalt oxide materials synthesized via ultrasonic spray pyrolysis. *J. Electrochem. Soc.* **2014**, *161*, A1338−A1349.
(43) Song, J.; Bazant, M. Z. Effects of nanoparticle geometry and size distribution on diffusion impedance of battery electrodes. *J. Electrochem. Soc.* **2013**, *160*, A15−A24.
(44) Patel, R. L.; Park, J.; Liang, X. Ionic and electronic conductivities of atomic layer deposition thin film coated lithium ion battery cathode particles. *RSC Adv.* **2016**, *6*, 98768−98776.
(45) Liu, J.; Manthiram, A. Functional surface modifications of a high capacity layered $Li[Li_{0.2}Mn_{0.54}Ni_{0.13}Co_{0.13}]O_2$ cathode. *J. Mater. Chem.* **2010**, *20*, 3961−3967.
(46) Huggins, R. A. Simple method to determine electronic and ionic components of the conductivity in mixed conductors a review. *Ionics* **2002**, *8*, 300−313.
(47) Liang, X.; Hakim, L. F.; Zhan, G.-D.; McCormick, J. A.; George, S. M.; Weimer, A. W.; Spencer, J. A.; Buechler, K. J.; Blackson, J.; Wood, C. J.; Dorgan, J. R. Novel processing to produce polymer/ceramic nanocomposites by atomic layer deposition. *J. Am. Ceram. Soc.* **2007**, *90*, 57−63.

DOI: 10.1021/acsomega.7b01922
ACS Omega 2018, 3, 906−916